Efficiencies of Electron Injection from Excited Sensitizer Dyes to Nanocrystalline ZnO Films as Studied by Near-IR Optical Absorption of Injected Electrons

Ryuzi Katoh,*,† Akihiro Furube,† Kohjiro Hara,† Shigeo Murata,† Hideki Sugihara,† Hironori Arakawa,† and M. Tachiya‡

Photoreaction Control Research Center (PCRC), National Institute of Advanced Industrial Science and Technology (AIST), Tsukuba Central 5, Tsukuba, Ibaraki 305-8565, Japan

Received: June 25, 2002; In Final Form: September 25, 2002

Near-IR absorption spectra of electrons injected from excited sensitizer dyes to nanocrystalline ZnO films have been studied. The absorption steeply increases with increasing wavelength and can be assigned to the optical transition of conducting electrons to higher energy levels of the conduction band. From the measurements in various sensitizer dyes, the relative efficiencies of the electron injection can be obtained as a function of the free energy change (ΔG) for the electron injection process. Around $\Delta G = 0$ eV, the efficiencies increase gradually with increasing $-\Delta G$ and they are constant at negative ΔG. We succeeded in explaining the tendency by considering the site heterogeneity of the surface. The relation between the injection efficiencies and the solar cell performance will also be discussed.

Introduction

Photocurrent assisted by the dye-sensitization of semiconductor electrodes was found in 1968.[1] Using this technique, visible light can be converted into electricity. The development of solar cells based on the dye-sensitization of the semiconductor electrode has been attempted by several groups. At that time, however, the solar-energy-to-electricity conversion efficiencies η were very low because only few molecules exist on the surface and almost all photons pass through the electrodes. In 1976, Tsubomura and co-workers succeeded in improving the light-harvesting efficiency using porous ZnO electrodes. They obtained high efficiency $\eta = 1.5\%$ at 563 nm light irradiation.[2] In 1993, Grätzel and co-workers made a remarkable improvement of the light harvesting efficiency using nanocrystalline TiO_2 film. They developed a highly efficient dye-sensitized solar cell (Grätzel cell) consisting of the N3 dye (*cis*-bis-(4,4′-dicarboxy-2,2′-bipyridine) dithiocyanato ruthenium(II); Ru(dcbpy)$_2$(NCS)$_2$) adsorbed on nanocrystalline TiO_2 films ($\eta =$ 10% under AM 1.5 irradiation).[3] In the past decade, much effort has been made to develop high performance solar cells based on this concept. However, the solar cell performance has not been improved remarkably. Thus, to find parameters controlling solar cell performance, the detailed mechanism of the solar cells has been studied extensively.

Figure 1 shows the primary steps of the dye-sensitized solar cells. Upon photoexcitation of the sensitizer dyes, the electrons are injected from the excited sensitizer dyes to the conduction band (CB) of the semiconductor film (electron injection). The injected electrons recombine with the oxidized sensitizer dyes (recombination). The recombination process is in competition with the rereduction of the oxidized sensitizer dyes by the redox mediator molecules (I^-/I_3^-) (rereduction). The remaining electrons can be transported in the semiconductor film as the conducting electrons. The conducting electrons are able to react with the redox mediator molecules during the transport before reaching the back contact electrode (dark current) and, finally, the remainder flow into the external circuit.

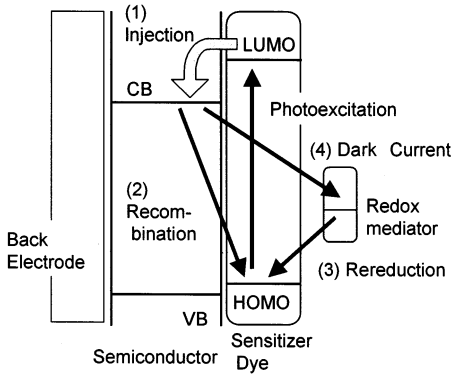

Figure 1. Primary reaction steps in dye-sensitized solar cells.

To realize high performance solar cells, the efficiency of the electron injection must be high. Therefore, the electron injection process can be considered to be one of the most important processes. To understand the injection process in detail, the dynamics and efficiency of the electron injection have been studied. From femtosecond transient absorption measurements, it has been reported that the electron injection occurs very rapidly within 0.1−100 ps time range in TiO_2,[4−11,16] ZnO,[12,13,16] and SnO_2.[14−16] The rate of the electron injection is much faster than that of the fluorescence decay of sensitizer dye which is typically 10 ns. Therefore, a high efficiency of the electron injection can be expected. However, it was reported that the efficiency of the electron injection depends on the identity of sensitizer dyes, whereas the rate of the electron injection is not sensitive to that.[16] This indicates that fast injection kinetics does not always lead to high efficiency. Anyway, the direct measurement of the injection efficiency is required to clarify the mechanism of solar cells.

The charge recombination occurs within millisecond time range in TiO_2[17−21] and in ZnO.[22] Therefore, all of the injected electrons are still alive in the nanosecond time range. Thus, the number of the injected electrons has been evaluated by

* To whom correspondence should be addressed. E-mail: r-katoh@aist.go.jp.
† PCRC, AIST.
‡ AIST.

10.1021/jp021484j CCC: $22.00
Published on Web 11/19/2002

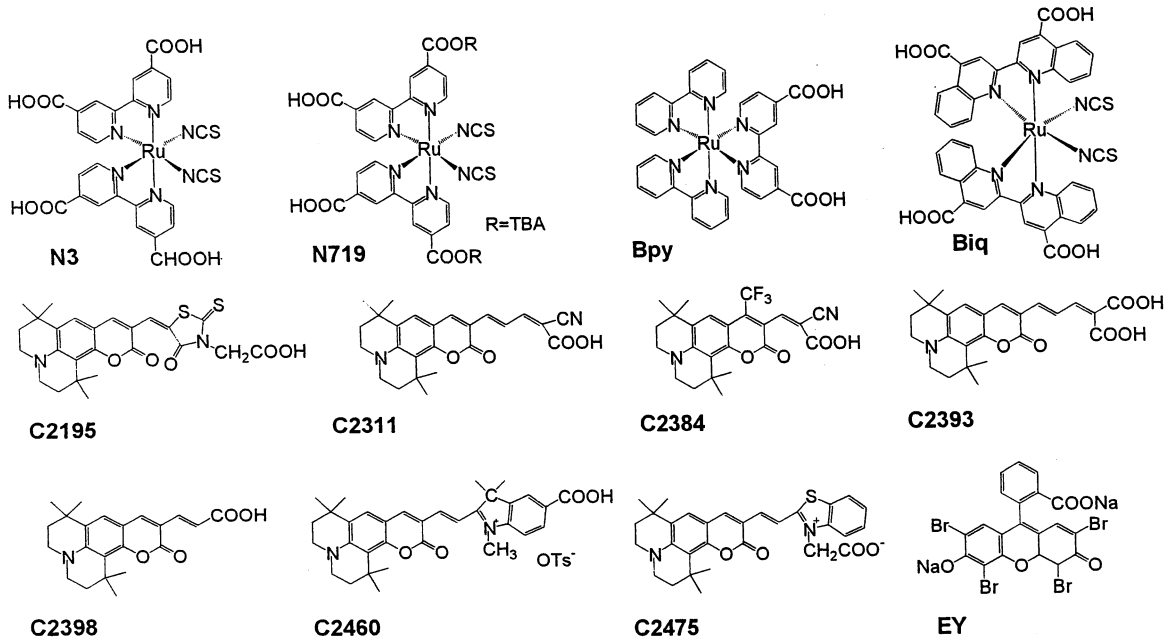

Figure 2. Molecular structure of sensitizing molecules studied.

nanosecond transient absorption spectroscopy. In a previous paper,[23] we studied the effect of the molecular structure of the sensitizer dye on the efficiency of the electron injection and found that it is strongly affected by the number of carboxyl groups involved in the sensitizer. From detailed analysis of the transient absorption spectra, we have concluded that this result can be attributed to the presence of inactive dyes on the TiO_2 surface, which are not effective for the electron injection.

Transient absorption measurements in these systems have been carried out mainly by observing the bleaching of the ground-state absorption of sensitizer dyes and the absorption because of excited and oxidized sensitizer dyes in the visible wavelength range (400−900 nm). These signals often overlap with each other. Therefore, the analysis of the spectra and decay profiles is not always easy.[10] Moreover, the assignment of the absorption band of newly synthesized sensitizer dyes is usually difficult. Thus, it is considered that the observation of electrons injected into the semiconductor film is more appropriate for detailed analysis, because in the near-IR wavelength range the absorption because of conducting electrons in semiconductor film is expected to appear without any overlapping with other absorption bands. The absorption because of injected electrons in the IR wavelength range has been observed to study dynamics of the electron injection process[9,10,13,16] and the loss process of conducting electrons during transport.[24]

The nanocrystalline TiO_2 film is considered to be the most promising material to realize high performance dye-sensitized solar cells. A nanocrystalline ZnO film has also been studied as a semicondcutor electrode for the dye-sensitized solar cells because the energy level of its conduction band (−0.2 V vs NHE at pH = 1) is similar to that of TiO_2 (−0.28 V vs NHE at pH = 2).[25] However, the performance of solar cells based on the N3-adsorbed nanocrystalline ZnO film is significantly lower than that of TiO_2 solar cells.[26−28] One of the reasons of the low performance of N3/ZnO has been attributed to the complex formation of N3 with Zn^{2+} ions on the ZnO film.[29] Recently, we have confirmed this idea through fluorescence microscopy and transient absorption spectroscopy.[30] We found that the low efficiency is due to the formation of micrometer-sized particles of the complex between N3 and Zn^{2+} ions, which are not effective for the electron injection. On the contrary, dye-sensitized solar cells using organic dyes as sensitizer molecules, such as eosin Y,[31] mercurochrome,[32] the solar cell performance of nanocrystalline ZnO system is similar to that of TiO_2 system. This also suggests that the low performance of the Ru-complex/ZnO cells is due to the complex formation. Thus, we believe that the nanocrystalline ZnO film is a promising material for high performance solar cells. We have studied the primary processes of ZnO systems in detail[30]

Here we report the near-IR absorption spectrum of electrons injected into nanocrsytalline ZnO films and relative efficiencies of the electron injection as a function of $-\Delta G$. To explain the $-\Delta G$ dependence, we take into account the site heterogeneity of semiconductor surfaces in the model of the electron injection. Moreover, we discuss the relation between the relative efficiency and the solar cell performance.

Experimental Section

A ZnO paste composed of ZnO nanoparticles (Sumitomo Osaka Cement, #100), polyvinyl acetal (Sekisui Kasei, BM-2), and α-terpineol was painted on a glass plate with a screen printer (Mitani Electronics Co., MEC-2400). Nanocrystalline films were prepared by calcination of the painted substrate for 1 h at 420 °C. The thickness of the films was about 5 μm, and the films were optically transparent. The apparent area of the ZnO films was about 1 cm^2 (1 cm × 1 cm). The sensitizer dyes were dissolved in dehydrated ethanol (Wako Chemicals) or *tert*-butyl alcohol (Kanto, G grade)-acetonitrile (Kanto, dehydrated) mixture solvent (50:50). These solvents were used without further purification. Figure 2 shows the molecular structures of sensitizer molecules studied. A detailed synthetic procedure of coumarin dyes has been reported elsewhere.[33] The sample specimens were prepared by immersion of the ZnO substrate into the dye solution. It has been reported that the formation of a complex between Ru-dye and Zn^{2+} proceeds with immersion time.[29,30] Therefore, the sample specimens were immersed into the dye solution only for 3 min at 25 °C to minimize complex formation on the ZnO films. The sample specimens dried in air were used for transient absorption measurements. All measurements were carried out just after preparation of the sample specimens to minimize the effect of dye degradation.

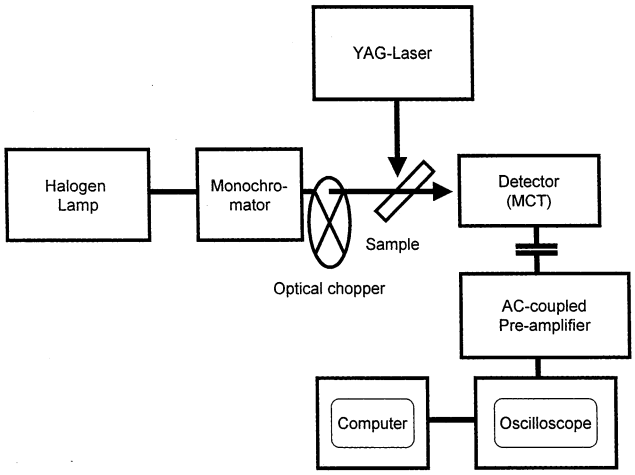

Figure 3. Near-IR transient absorption spectrometer constructed.

Figure 3 shows the diagram of a transient absorption spectrometer constructed. This is similar to the transient infrared-spectrometer constructed by Hamaguchi and co-workers.[34] A Nd^{3+}:YAG laser (HOYA Continuum, Surelite II) was used for the pumping light source. The repetition rate of the laser was 10 Hz. The third harmonic pulse (355 nm) and the second harmonic pulse (532 nm) were used for the excitation of naked and a dye-sensitized ZnO films, respectively. A halogen lamp (50 W) was used as the probe light source. The probe light was dispersed with a monochromator (ACTON, SpectraPro-150) and was incident at 45° on the sample specimen. The transmitted light was detected with a MCT-photodetector (Dorotek, PDI-2TE−4). The photocurrent from the detector was amplified with an AC-coupled preamplifier (NF Electronic Instruments, SA-230F5) and a differential amplifier (NF Electronic Instruments, 5305). Signals were processed with a digital oscilloscope (Tektronix, TDS680C) and analyzed with a computer. Using the preamplifier, the DC offset of the photocurrent from the detector can be subtracted, and therefore, a small absorbance change ($<10^{-5}$) can be detected. The time resolution of the system was about 50 ns. To calculate the absorbance change, the intensity of the probe light without laser excitation was required, and it was measured by modulating the probe light intensity with an optical chopper placed in front of the detector. All measurements were carried out at room temperature.

Results and Discussion

Near-IR Transient Absorption Spectrum. The band gap of ZnO was reported as 3.0−3.2 eV.[25] Therefore, electrons and holes are produced in ZnO upon 355 nm ($h\nu = 3.49$ eV) light excitation. The bottom curve in Figure 4 shows the transient absorption spectrum of a naked ZnO nanocrystalline film just after excitation with 355 nm light pulse. The shape of the spectrum did not change with time. The absorbance increases steeply with increasing wavelength, which is characteristic of the conducting electron in semiconductors, i.e., the optical transition from free electrons in the bottom of a conduction band (or shallow trapped electrons) to upper levels of the conduction band.[35] According to the theoretical consideration for an ideal crystal, the shape of the spectrum can be reproduced by the power law λ^n with $n = 0.5-3.5$.[35] The factor n was found to be $n = 2-3.5$ in several semiconductor crystals[35] and $n = 3.5$ for TiO_2 nanoparticles.[36] However, the spectrum of a naked nanocrystalline ZnO film shown in Figure 4 is fitted with $n = 4.5$. This discrepancy with the model may be due to the deviation of the shape of the conduction band from a parabolic shape which is expected in an ideal crystal.

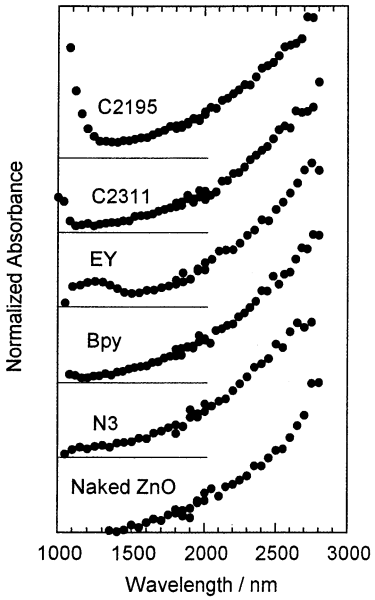

Figure 4. Transient absorption spectra of the naked ZnO film (bottom) and the ZnO film sensitized by N3, Bpy, EY, C2311, and C2195.

We also measured the near-IR transient absorption spectra of nanocrystalline ZnO films sensitized by N3, Bpy, EY, C2311, and C2195 (Figure 4). These spectra are similar to that of naked ZnO film. Below 1200 nm, a small peak in EY/ZnO and an absorption tail in C2195/ZnO and C2311/ZnO were detected. In the case of EY, the absorption peak of the triplet excited state was observed at 1 040 nm in solution.[37] Therefore, we tentatively assigned the peak around 1 200 nm to the T−T absorption of EY adsorbed on the film. This peak decays in a manner similar to that of the injected electron observed around 2 500 nm, suggesting that the triplet excited sensitizer dyes are equilibrated with the charge-separated state (dye-cation and conducting electron). Similar observation was reported in all *trans*-retinoic acid adsorbed on TiO_2 colloid.[38] For C2195 and C2311, we cannot assign the absorption band below 1 200 nm because no transient absorption spectra data are available for these compounds in solution.

Relative Efficiency of the Electron Injection. The absorbance change induced by the production of electrons in the near-IR wavelength range is proportional to the number of electrons injected by light irradiation. Thus, the relative efficiencies of the electron injection can be evaluated, if all measurements can be carried out under the same optical geometry and a correction is made for the number of absorbed photons. To obtain the efficiencies, the decay profiles have to be measured precisely. It is well-known that the rate of the charge recombination in nanocrystalline films is very sensitive to excitation intensity I_{ex}.[18,19] Figure 5 shows the decay profile of the transient absorption observed at 2 500 nm. The decay for the 280 μJ cm^{-2} excitation is faster than that for 35 μJ cm^{-2} excitation. At early times, the signal for the 280 μJ cm^{-2} excitation seems to decay very fast, although the very fast decay cannot be detected with our apparatus. Figure 6 shows the apparent efficiency evaluated from the absorbance at time zero of the decay profiles, as a function of I_{ex}. The apparent efficiencies decrease with increasing I_{ex}. Thus, we recorded the decay profiles for excitation below 100 μJ cm^{-2} to evaluate the efficiencies. Under this condition, the decay profiles are not affected by the light intensity. As we mentioned, the correction for the number of absorbed photons

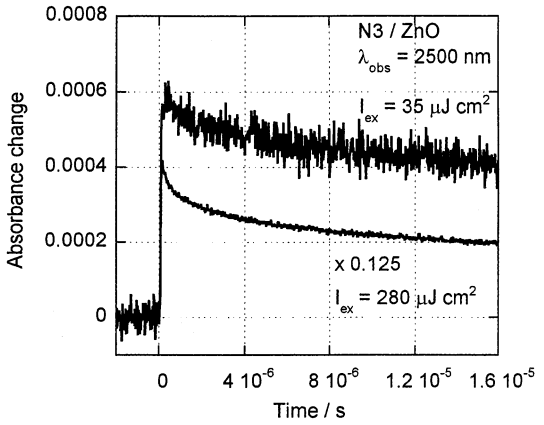

Figure 5. Temporal profiles of transient absorption of the N3/ZnO film observed at 2 500 nm at $I_{ex} = 35\ \mu J\ cm^{-2}$ and $I_{ex} = 280\ \mu J\ cm^{-2}$. The decay profiles are normalized by exciting light intensities.

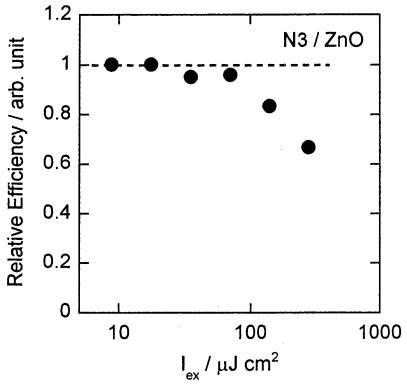

Figure 6. Relative efficiencies of the electron injection as a function of exciting light intensity.

is another important factor for accurate evaluation of the efficiencies. We estimate that from the absorption spectra of the films after correction of light scattering. For Bpy and C2398, the experimental error is significantly large because of the small absorbance of the ground-state absorption at 532 nm.

The free energy change ΔG_{exp} obtained experimentally can be expressed as

$$-\Delta G_{exp} = eE_{CB}^{ZnO} - eE_{OX}^{dye*} \quad (1)$$

where E_{CB}^{ZnO} is the reduction potential of the bottom of the conduction band of ZnO and E_{OX}^{dye*} is the oxidation potential of the sensitizer dye in the excited state. It was reported that E_{CB}^{ZnO} depends on pH of the solvent, $E_{CB}^{ZnO} = -0.2$ V at pH = 1 and -0.4 V at pH = 4.8 vs NHE.[25] We assume that the effective pH of the dried specimen is pH = 7 and estimate $E_{CB}^{ZnO} = -0.5$ V at pH = 7 by extrapolation of the reported values. When we evaluate the E_{OX}^{dye*}, we consider two cases. In one case, the electron injection occurs before relaxation, namely, from the Franck−Condon state of optical excitation. In the other case, it occurs after relaxation, namely, from the lowest vibrational state in the excited state. In the former case, the injection occurs from the energy level reached upon photoexcitation. Therefore, $E_{OX}^{dye*}(532)$ can be expressed as

$$E_{OX}^{dye*}(532) = eE_{OX}^{dye} - h\nu_{exc} \quad (2)$$

where E_{OX}^{dye} is the oxidation potential of the sensitizer dyes in the ground state and $h\nu_{exc}$ is the exciting photon energy. In the present study, excitation was made at 532 nm photon ($h\nu_{exc} =$ 2.33 eV). The electron injection from unrelaxed higher excited states has been observed through femtosecond transient absorption spectroscopy in the TiO_2 system[11] and subpicosecond fluorescence spectroscopy in the SnO_2 system[14] and the photocurrent action spectrum in TiO_2.[39] On the other hand, the electron injection from the relaxed state is also observed. In this case, $E_{OX}^{dye*}(0-0)$ can be expressed as

$$E_{OX}^{dye*}(0-0) = eE_{OX}^{dye} - E_{0-0} \quad (3)$$

where E_{0-0} is the energy of the relaxed excited state, which can be obtained from the onset energy of the ground-state absorption. In the case of the Ru complex, intersystem crossing from the singlet excited state to the triplet excited state is known to be very fast, which is comparable to the relaxation from the higher excited state. Therefore, the onset energy of the emission from the triplet state is used as E_{0-0}. In Table 1, the oxidation potentials (vs NHE) and the E_{0-0} of sensitizer dyes studied are listed.

TABLE 1: Redox Potentials and Absorption Edge of the Dyes

no.	compnd	Φ_{inj}^{rel} [a] eV	E_{OX}^{dye} [b] V	E_{0-0} [c] eV	$-\Delta G_{exp}^{532nm}$ [d] eV	$-\Delta G_{exp}^{0-0}$ [e] eV
1	N3	1.0	1.06[f]	1.91[f]	0.77	0.35
2	N719	1.0	0.91[f]	1.91[f]	0.92	0.50
3	Bpy	1.2	1.52[g]	2.25[h]	0.31	0.23
4	Biq	0.15	1.16[i]	1.53[i]	0.67	−0.13
5	C2195	0.45	1.22[j]	1.85[j]	0.61	0.13
6	C2311	0.85	1.28[j]	1.95[j]	0.55	0.17
7	C2384	0.40	1.46[j]	1.98[j]	0.37	0.02
8	C2393	0.8	1.16[j]	2.07[j]	0.67	0.40
9	C2398	1.1	1.20[j]	2.25[j]	0.63	0.55
10	C2460	0.4	1.18[j]	1.68[j]	0.65	−0.01
11	C2475	0.4	1.15[j]	1.63[j]	0.68	−0.02
12	EY	0.65	1.10[k]	2.10[l]	0.73	0.50

[a] Relative efficiency of the electron injection normalized by the value of N3. [b] Oxidation potential in the ground state (vs NHE). [c] Energy of relaxed excited state. [d] Free energy change estimated using eq 2. [e] Free energy change estimated using eq 3. [f] Reference 40. [g] Reference 41. [h] Reference 42. [i] Reference 43. [j] Reference 33. [k] Reference 44. [l] Reference 31.

Figure 7, parts a and b, shows the relative efficiencies Φ_{inj} of the electron injection as a function of $-\Delta G_{exp}$ calculated by eqs 2 and 3, respectively. It was reported that the low loading N3/ZnO film has a high value of IPCE (the incident photon-to-current conversion efficiency),[29] suggesting that the efficiencies of the electron injection is almost unity. Thus, the efficiencies are normalized at the value for N3. There seems to be no correlation between Φ_{inj} and $\Delta G(532)$ in Figure 7a, whereas a good correlation can be seen in Figure 7b. This indicates that the electron injection occurs from the relaxed excited state of the sensitizer dyes on ZnO. As shown in Figure 7b, the relative efficiencies Φ_{inj} increases with increasing $-\Delta G_{exp}$ around $-\Delta G_{exp} = 0$ eV, and they are constant at negative ΔG.

Model of the Electron Injection from Excited Dyes to Nanocrystalline Films. We shall consider the model of the electron injection from excited sensitizer dyes to nanocrystalline film to understand the $-\Delta G$ dependence. For electron transfer reactions in solution, many theories, such as the Marcus theory, have been proposed, and they were successfully applied to many actual systems. In the present system, namely, dye-sensitized nanocrystalline semiconductor films dried in air, the conditions for electron-transfer reactions are different from those in solution. Actually, the acceptor level (conduction band of the semiconductor) is a continuum, and no solvation process can be induced by solvent reorganization.

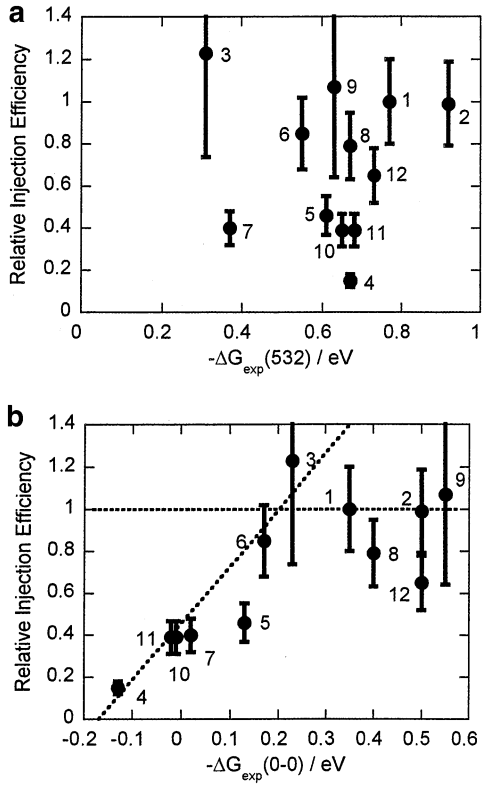

Figure 7. Relative efficiencies of the electron injection as a function of $-\Delta G_{exp}$. The $-\Delta G_{exp}$ is evaluated by considering two cases, (a) electron injection before relaxation (eq 2) and (b) after relaxation (eq 3). Numbers in the figure represent the compounds listed in Table 1.

Sakata and co-workers studied the electron-transfer process in dye-adsorbed semiconductor powder crystal by picosecond time-resolved fluorescence spectroscopy[45] and proposed a model of the electron injection process from excited dyes to the conduction band of the semiconductor.[46] They assumed an ideal system, namely, no reorganization energy and parabolic conduction band. Although multiexponential decay of fluorescence was observed, they evaluated the electron injection rate constant from the fastest decay component which is the main decay component. They successfully explained the dependence of the injection rate on the free energy change using the proposed model. In the dye-sensitized nanocrystalline semiconductor system, multiexponential kinetics of the electron injection has been observed through ultrafast spectroscopy in TiO_2,[4−11,16] ZnO,[12,13,16] and SnO_2.[14−16] It was found that the deviation from exponential kinetics is more significant than in powder crystals. This may be due to morphology difference between nanocrystalline films and powder crystals, suggesting that the model proposed by Sakata et al.[46] is difficult to apply to the present systems. We have to take into account the energy distribution originating from the site heterogeneity explicitly. Tachibana et al. presented the model including the site heterogeneity to explain the kinetics of the electron injection.[7] The model cannot apply directly to discuss the efficiency of the injection as a function of $-\Delta G$.

The energy distribution may be due to morphology of the surface. It was reported that the energy level of the conduction band edge depends on the crystal face. The conduction band edge of the anatase (101) face of TiO_2 is shifted negatively by 0.2 V relative to that of the rutile (001) face.[47] For nanocrystalline films, many crystal faces as well as crystal structures exist at the surfaces. Therefore, ΔG of the electron injection is different from site to site. Recently, Lu and Xie studied

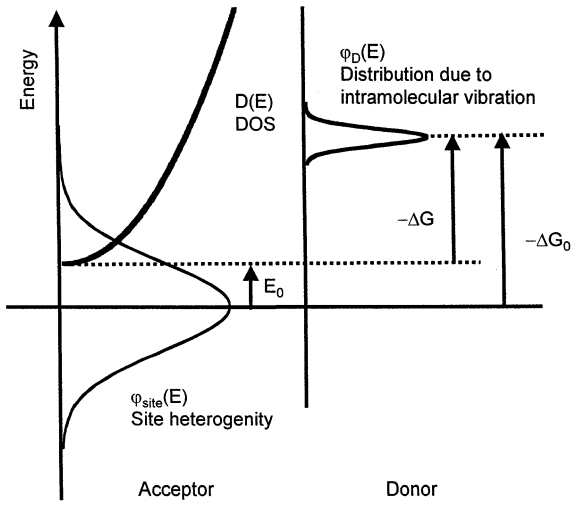

Figure 8. Energy level diagram for the model of electron injection at semiconductor surface. $\varphi_D(E)$ and $\varphi_{site}(E)$ represent the distribution because of intramolecular vibration and the site heterogeneity, respectively. D(E) represents the density of state of the ideal crystal. ΔG is the free energy change of the electron injection at a given site, and ΔG_0 is the peak energy of the distribution of the free energy change because of site heterogeneity.

microscopic phenomena of electron-transfer reactions by using a single molecule fluorescence technique for organic dyes on ITO films.[48] According to their study, each molecule shows single-exponential decay but the lifetimes are different from site to site. On the other hand, multiexponential decay was observed in conventional fluorescence decay measurements. This indicates that site heterogeneity is essential to explain multiexponential kinetics for the electron injection process at interfaces.

The rate constant k_{ET} of the electron injection can be expressed generally as[49]

$$k_{ET} = \frac{2\pi}{\hbar} J^2 \int_{-\infty}^{+\infty} \Psi_i(E)\, \Psi_f(E)\, dE \qquad (4)$$

where J is the transfer integral (the electronic coupling matrix element for the electron-transfer reaction) and $\psi_i(E)$ and $\psi_f(E)$ are the electron detachment spectrum and the electron attachment spectrum, respectively.[49] The transfer integral decreases exponentially with increasing distance d between the donor and the acceptor as

$$J = J_0 \exp(-\beta d) \qquad (5)$$

where J_0 is the value at $d = 0$ and β is constant and estimated as $\beta = 1$ Å^{-1}.[50] In the present system, the donor molecule is attached to the acceptor surface tightly through the carboxyl group as an anchor. Thus, the distance between the donor and the acceptor can be considered to be constant. Therefore, J is also constant. Figure 8 illustrates the energy level diagram of the donor and the acceptor for the electron injection process at the interface in the presence of site heterogeneity. The energy distribution $\varphi_D(E)$ of the excited sensitizer dye originates from the intramolecular vibrations of the sensitizer dye. In the present system, there is no solvent molecule. Therefore, the energy distribution originating from the surrounding solvent molecules can be neglected. The electron injection occurs from the donor state to the conduction band of the ZnO film. The density of states (DOS) of the conduction band is represented by D(E) and has the distribution originating from the site heterogeneity $\varphi_{site}(E)$. These energy distributions can be expressed as

$$\varphi_{\mathrm{D}}(E) = \frac{1}{(4\pi k_{\mathrm{B}} T \lambda_{\upsilon})^{1/2}} \exp\left[-\frac{(E + \Delta G_0 + \lambda_{\upsilon})^2}{4 k_{\mathrm{B}} T \lambda_{\mathrm{v}}}\right] \quad (6)$$

$$D(E) = \frac{1}{2\pi^2}\left(\frac{2m}{\hbar^2}\right)^{3/2}\sqrt{E - E_0} \quad (7)$$

$$\varphi_{\mathrm{site}}(E) = \frac{1}{(2\pi\sigma_{\mathrm{site}}{}^2)^{1/2}} \exp\left[-\frac{E^2}{2\sigma_{\mathrm{site}}{}^2}\right] \quad (8)$$

where λ_{υ} is the reorganization energy due to the intramolecular vibration of the sensitizer dyes, m is the effective mass of the electron in the semiconductor, and σ_{site} is the parameter for site heterogeneity. The free energy change ΔG of the electron injection can be defined as the energy difference between the bottom of the conduction band and the energy of an excited sensitizer dye at a given site, and ΔG_0 is the peak energy of the distribution of the free energy change because of site heterogeneity. Thus, ΔG_0 corresponds to the free energy change ΔG_{exp} estimated experimentally (see eq 1).

For the calculation of the rate constant k_{ET} of the electron injection at a given site, $\varphi_{\mathrm{D}}(E)$ can be used as the electron detachment spectrum $\Psi_{\mathrm{i}}(E)$ and $D(E)$ can be used as the electron attachment spectrum $\Psi_{\mathrm{f}}(E)$. For the calculation of k_{ET} of the actual specimen, the distribution due to the site heterogeneity has to be averaged. In this case, k_{ET} is the function of E and ΔG_0. In the present system, we assume that the geometrical structure of adsorbed sensitizer dyes on the surface are fixed; that is, the energy distribution $\varphi_{\mathrm{site}}(E)$ due to site heterogeneity is frozen. On the contrary, as shown in Figure 7, the electron injection occurs after vibrational relaxation. Therefore, the energy fluctuation due to intramolecular vibrational motion can be considered to be faster than the electron injection. Under this condition, the kinetics of the electron injection is represented by the superposition of single-exponential kinetics at each site. Therefore, the survival probability of the electron injection can be expressed as

$$P(t) = \exp[-k_{\mathrm{f}} t] \int_{-\infty}^{+\infty} \exp[-k_{\mathrm{ET}}(E,\Delta G_0)t]\varphi_{\mathrm{site}}(E)\, \mathrm{d}E \quad (9)$$

where k_{f} is the rate constant of fluorescence decay. The efficiency Φ_{inj} of the electron injection can be written as follows:

$$\Phi_{\mathrm{inj}}(\Delta G_0) = \int_{-\infty}^{+\infty} \frac{k_{\mathrm{ET}}(E,\Delta G_0)}{k_{\mathrm{f}} + k_{\mathrm{ET}}(E,\Delta G_0)} \varphi_{\mathrm{site}}(E)\, \mathrm{d}E \quad (10)$$

It should be emphasized that the energy distribution $\varphi_{\mathrm{site}}(E)$ of the free energy changes at different sites is important to explain the multiexponential kinetics of the electron injection. If the energy fluctuation in this distribution is much faster than that of the electron injection rate, the survival probability P(t) can be expressed as

$$P(t) = \exp[(-k_{\mathrm{f}} + k_{\mathrm{ET}}(\Delta G_0))t] \quad (11)$$

In this case, the kinetics of the electron injection can be fitted by a single exponential function. The efficiency of the electron injection can be expressed simply as

$$\Phi_{\mathrm{inj}}(\Delta G_0) = \frac{k_{\mathrm{ET}}(\Delta G_0)}{k_{\mathrm{f}} + k_{\mathrm{ET}}(\Delta G_0)} \quad (12)$$

The conventional relation described above has been widely used to estimate the injection efficiency. However, this relation cannot be applied to the system which shows multiexponential kinetics, such as electron injection process in nanocrystalline film.

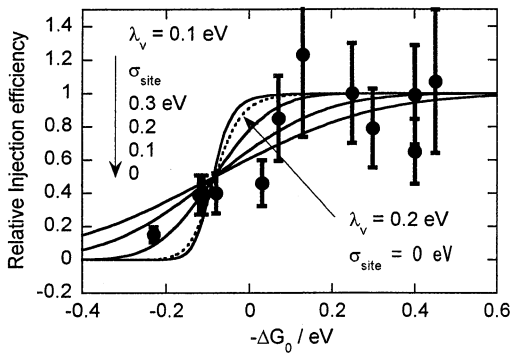

Figure 9. Relative injection efficiency as a function of $-\Delta G_0$, using the values $\lambda_{\mathrm{v}} = 0.1$ eV and $\sigma_{\mathrm{site}} = 0$, 0.1, 0.2, and 0.3 eV (solid line) and $\lambda_{\mathrm{v}} = 0.2$ eV and $\sigma_{\mathrm{site}} = 0$ eV (dotted line). The experimental data are plotted using the relation; $-\Delta G_0 = \Delta G_{\mathrm{exp}} - 0.1$.

The efficiency of the electron injection as a function of $-\Delta G_0$ can be evaluated using eq 10. We assume the reorganization energy due to intramolecular vibrations λ_{v} equals 0.1 eV, which is typical value of the intramolecular vibrational energy. To evaluate the efficiencies of the electron injection, we assume the rate constant at $-\Delta G = 0.35$ eV to be $k_{\mathrm{ET}} = 10^{11}$ s^{-1} because it was reported that the injection from N3 occurs within 1−10 ps time range.[13] For comparison with the experimental data, the rate constants k_{f} of fluorescence decay of sensitizer dyes are required. However, the rate constants of the fluorescence decay differ from one dye to another's, for example $k_{\mathrm{f}}^{-1} = 2$ ns for C2311[33] and $k_{\mathrm{f}}^{-1} = 25$ ns for N3.[4] To obtain the tendency of the dependence of the efficiencies on $-\Delta G_0$, we assume $k_{\mathrm{f}}^{-1} = 10$ ns for all dyes considered.

Figure 9 shows the results of the calculation of the efficiencies using the values $\lambda_{\mathrm{v}} = 0.1$ eV and $\sigma_{\mathrm{site}} = 0$, 0.1, 0.2, and 0.3 eV by solid lines and $\lambda_{\mathrm{v}} = 0.2$ eV and $\sigma_{\mathrm{site}} = 0$ eV by dotted line. To compare the experimental data with the model calculation, we assume the relation; $-\Delta G_0 = -\Delta G_{\mathrm{exp}} - 0.1$ eV. The difference may be due to oversimplification of the method for estimating $-\Delta G_{\mathrm{exp}}$. The shape of the injection efficiency seems to be not sensitive to λ_{v}. As shown in Figure 9, the efficiency increases steeply for no site heterogeneity ($\sigma_{\mathrm{site}} = 0$ eV), whereas the experimental data increases gradually with increasing $-\Delta G_0$. This clearly indicates that the $-\Delta G_0$ dependence cannot explain the effect of the reorganization due to intramolecular vibration. The calculation including site heterogeneity is required to explain the tendency of the injection efficiency. The experimental data are scattered between the curve for $\sigma_{\mathrm{site}} = 0.1$ eV and that for 0.2 eV. Thus, $\sigma_{\mathrm{site}} = 0.15$ eV seems to represent the experimental tendency. It increases gradually between −0.4 and 0.2 eV with increasing $-\Delta G_0$, and above 0.2 eV, it tends to saturate. It should be emphasized that site heterogeneity is important to explain the gradual increase of the efficiencies around $-\Delta G_0 = 0$ eV. According to our model, the gradual increase of the efficiency around $-\Delta G_0 = 0$ eV reflects site heterogeneity. At this $-\Delta G_0$ value, some excited molecules have positive $-\Delta G$ values and undergo the injection, whereas the other have negative $-\Delta G_0$ values and decay to the ground state.

We shall discuss the relation between site heterogeneity and electron traps. The site heterogeneity at surfaces produces traps for electrons, which is important to understand the mobility of an electron in nanocrystalline semiconductor films.[51] It has been reported that the absorption spectra of sensitizer dyes do not change by adsorption to nanocrystalline semiconductor films, suggesting that the electronic state is not affected by the

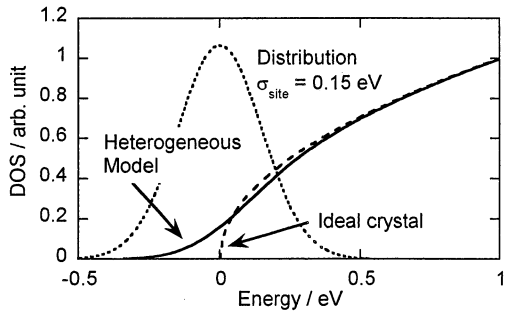

Figure 10. Density of states (DOS) of the ZnO film calculated from the convolution of ideal DOS function and site heterogeneity. Distribution because of site heterogeneity is plotted as the dotted line (σ_{site} = 0.15 eV). DOS of ideal crystal is shown by the dashed line.

adsorption. Moreover, the geometries of adsorbed dyes on semiconductor surfaces can be considered to be similar to each other because the sensitizer dyes are attached to the surface tightly through carboxyl group as an anchor. Therefore, it is considered that the site heterogeneity is due to the energy distribution of the conduction band edge, which is caused by difference in crystal structure and crystal face. Thus, the shape of the DOS for nanocrystalline semiconductor film may be expressed as the superposition of the DOS for each site. The solid line in Figure 10 shows the DOS obtained by the convolution of the site heterogeneity with the value of σ_{site} = 0.15 eV (dotted line) and the DOS of ideal crystal (dashed line). In nanocrystallne films, DOS is extended up to negative E values, whereas in ideal crystals, it abruptly starts at $E = 0$. Above $E = 0$ eV, however, the shape of the DOS for nanocrystalline film is similar to that for the ideal crystal. The DOS below $E = 0$ eV may act as traps for electrons.

The distribution D_{trap} of the depths of trap sites in nanocrystalline semiconductors is usually assumed to be exponential

$$D_{trap} = A \exp\left(-\frac{E}{E_{tail}}\right) \tag{13}$$

where A is the constant and E_{tail} is a characteristic parameter for the exponential distribution. It has been reported that the value of E_{tail} is found to be between 0.06 and 0.2 eV in nanocrystalline TiO_2 films through electrochemical measurements.[52,53] The distribution can also be evaluated through the analysis of the recombination kinetics, which reflects the diffusion process of electrons limited by the trapping-detrapping events. Recently, Barzykin and Tachiya analyzed the recombination kinetics in nanocrystalline TiO_2 films by using a random flight model.[51] One of the fitting parameters of the model is the distribution of trap depth. They found E_{tail} to be 0.06 eV, and it is similar to that from experimental results (0.06−0.2 eV). According to the study by Durrant and coworkers, the recombination kinetics of dye-sensitized ZnO films is similar to that in TiO_2.[22] This implies that the trap distribution in the ZnO film is similar to that in TiO_2. Figure 11 shows $D_{trap}(E)$ normalized at 0 eV with the values of E_{tail} = 0.06 and 0.2 eV and the tail of the $D(E)$ below 0 eV calculated using the value of σ_{site} = 0.15 eV. The distribution $D(E)$ estimated from the analysis of the efficiencies of the electron injection is similar to that evaluated from the analysis of electrochemical measurements and recombination kinetics in TiO_2 films. Trap distribution can be evaluated on the basis of site heterogeneity estimated from the efficiency of the electron injection, suggesting that site heterogeneity is very important to characterize the property of dye-sensitized nanocrystalline systems.

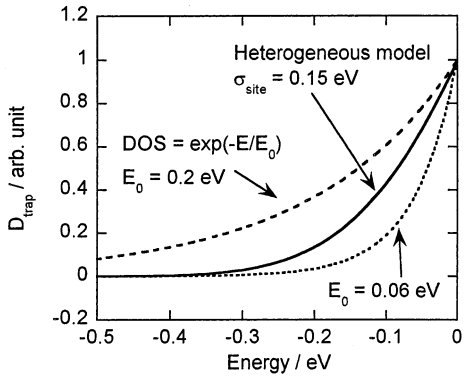

Figure 11. Distributions of the depths of traps estimated from the analysis of the recombination kinetics (E_0 = 0.06 eV, dashed line) and electrochemical measurements (E_0 = 0.06 and 0.2 eV, dashed and dotted lines) and from the analysis of the efficiencies of the electron injection using the value of σ_{site} = 0.15 eV (full line).

Relation between the Efficiency of Electron Injection and the Solar Cell Performance. As we mentioned, the electron injection process is one of the most important steps in the primary processes of the dye-sensitized solar cells. It is important to elucidate the relation between the solar cell performance and the efficiency of the electron injection. ZnO is a promising material for high performance solar cells because the energy level of the conduction band is similar to that of TiO_2. However, the solar cell performance is remarkably low for the N3/ZnO system,[26−28] although N3/TiO_2 system shows the highest performance.[3] The reason for the difference between the TiO_2 and ZnO systems has been studied, and it was concluded that the aggregates formed between N3 dyes and Zn^{2+} ions are responsible for the lower performance of the ZnO system.[29,30] In the present study, we used a diluted film. In other words, the dye concentration in our film is much lower than that in the actual solar cell devices. Thus, the aggregation can be ruled out. As shown in Figure 7, the efficiency of the electron injection from N3 into ZnO shows a relatively high value compared with other sensitizer dyes. This indicates that N3 has a higher potential for injecting an electron under the condition of no aggregation. Hagfeldt et al. reported that the solar cell performance of N3/ZnO can be significantly improved by changing countercations from proton to TBA,[29] i.e., N719 dye. As shown in Figure 7, the relative injection efficiency for N3 is the same as that for N719, suggesting that the electron injection ability of N3 is the same as that of N719 under the condition of no aggregation.

The energy level of the conduction band of ZnO is similar to that of TiO_2. Thus, we shall compare the $-\Delta G$ dependence of the efficiencies of the electron injection for ZnO system with the incident photon-to-current conversion efficiency (IPCE) in the dye-sensitized solar cells based on TiO_2. The relation between the IPCE at 532 nm in TiO_2 system and the efficiency of the electron injection in ZnO system is shown in Figure 12. The values of IPCE are collected from the previous results of N3,[40] N719,[40] Bpy,[54] Biq,[43] EY,[31] and coumarin dyes.[33] Figure 12 shows a good correlation between the two quantities, suggesting that the IPCE is limited by the electron injection process.

Many efforts have been made to synthesize new sensitizer dyes to realize high performance solar cells. The energy matching between E_{ox}^{dye*} and E_{CB} is important for high performance. Combining the relation between IPCE and the efficiency of the electron injection (Figure 12) with the $-\Delta G$ dependence of the efficiency of the electron injection (Figure 7), IPCE is

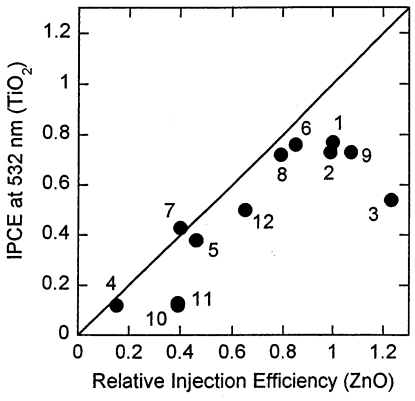

Figure 12. Relation between the IPCE at 532 nm of dye-sensitized TiO_2 solar cells and the efficiency of the electron injection in dye-sensitized ZnO films.

predicted to decrease gradually with decreasing $-\Delta G$ around $-\Delta G = 0$ eV. This indicates that $-\Delta G > 0.2$ eV is required to realize high performance solar cells.

Conclusion

We succeeded in measuring the near-IR absorption spectra of electrons injected from the excited dyes into ZnO nanocrystalline films. From the measurements on various dyes, the $-\Delta G$ dependence of the relative efficiency of the electron injection was obtained. Around $\Delta G = 0$ eV, the efficiencies increase gradually with increasing $-\Delta G$, and they are constant at negative ΔG. We proposed the model of electron transfer in which site heterogeneity was properly taken into account. Our model explained the results using the site distribution energy with $\sigma_{site} = 0.15$ eV. By comparing the solar cell performance in the TiO_2 system with the present results, we conclude that IPCE is limited by the efficiency of the electron injection.

Acknowledgment. We acknowledge Drs. Y. Tachibana, K. Seki and A. V. Barzykin for helpful discussion. We are grateful to Prof. J. R. Durrant for informing us of his experimental results on the recombination kinetics of ZnO film prior to publication. We are also grateful to Dr. S. Suga (Hayashibara Biochemical Laboratories) for synthesis of coumarin dyes. This work was supported by COE development program of MEXT of Japan.

References and Notes

(1) Gerischer, H.; Tributsch, H. *Ber. Bunsen-Ges. Phys. Chem*. **1968**, *72*, 437−445.
(2) Tsubomura, H.; Matsumura, M.; Nomura, Y.; Amamiya, T. *Nature* **1976**, *261*, 402−403.
(3) Nazeeruddin, M. K.; Kay, A.; Rodicio, I.; Humphry-Baker, R.; Muller, E.; Liska, P.; Vlachopoulos, N.; Grätzel, M. *J. Am. Chem. Soc*. **1993**, *115*, 6382−6390.
(4) Tachibana, Y.; Moser, J. E.; Grätzel, M.; Klug, D. R.; Durrant, J. R. *J. Phys. Chem*. **1996**, *100*, 20056−20062.
(5) Tachibana, Y.; Haque, S. A.; Mercer, I. P.; Durrant, J. R.; Klug, D. R. *J. Phys. Chem. B* **2000**, *104*, 1198−1205.
(6) Tachibana, Y.; Haque, S. A.; Mercer, I. P.; Moser, J. E.; Klug, D. R.; Durrant, J. R. *J. Phys. Chem. B* **2001**, *105*, 7424−7431.
(7) Tachibana, Y.; Rubtsov, I. V.; Montanari, I.; Yoshihara, K.; Klug, D. R.; Durrant, J. R. *J. Photochem. Photobio. A* **2001**, *142*, 215−220.
(8) Hannappel, T.; Burfeindt, B.; Storck, W.; Willig, F. *J. Phys. Chem. B* **1997**, *101*, 6799−6802.
(9) Asbury, J. B.; Ellingson, R. J.; Ghosh, H. N.; Ferrere, S.; Nozik, A. J.; Lian, T. *J. Phys. Chem. B* **1999**, *103*, 3110−3119.
(10) Benkö, G.; Hilgendorff, M.; Yartsev, A. P.; Sundström, V. *J. Phys. Chem. B* **2001**, *105*, 967−974.
(11) Benkö, G.; Kallioinen, J.; Korppi-Tommola, J. E. I.; Yartsev, A. P.; Sundström, V. *J. Am. Chem. Soc.* **2002**, *124*, 489−493.
(12) Bauer, C.; Boschloo, G.; Mukhtar, E.; Hagfeldt, A. *J. Phys. Chem. B* **2001**, *105*, 5585−5588.
(13) Asbury, J. B.; Wang, Y.; Lian, T. *J. Phys. Chem. B* **1999**, *103*, 6643−6647.
(14) Iwai, S.; Hara, K.; Murata, S.; Katoh, R.; Sugihara, H.; Arakawa, H. *J. Chem. Phys*. **2000**, *113*, 3366−3373.
(15) Kamat, P. V.; Bedja, I.; Hotchandani, S.; Patterson, L. K. *J. Phys. Chem*. **1996**, *100*, 4900−4908.
(16) Asbury, J. B.; Hao, E.; Wang, Y.; Ghosh, H. N.; Lian, T. *J. Phys. Chem. B* **2001**, *105*, 4545−4557.
(17) O'Regan, B.; Moser, J.; Anderson, M.; Grätzel, M. *J. Phys. Chem*. **1990**, *94*, 8720−8726.
(18) Haque, S. A.; Tachibana, Y.; Willis, R. L.; Moser, J. E.; Grätzel, M.; Klug, D. R.; Durrant, J. R. *J. Phys. Chem. B* **2000**, *104*, 538−547.
(19) Heimer, T. A.; Heilweil, E. J.; Bignozzi, C. A.; Meyer, G. J. *J. Phys. Chem. A* **2000**, *104*, 4256−4262.
(20) Haque, S. A.; Tachibana, Y.; Klug, D. R.; Durrant, J. R. *J. Phys. Chem. B* **1998**, *102*, 1745−1749.
(21) Kuciauskas, D.; Freund, M. S.; Gray, H. B.; Winkler, J. R.; Lewis, N. S. *J. Phys. Chem. B* **2001**, *105*, 392−403.
(22) Willis, R. L.; Olson, C.; O'Regan, B.; Lutz, T.; Nelson, J.; Durrant, J. R. *J. Phys. Chem. B* **2002**, *106*, 7605−7613.
(23) Hara, K.; Horiuchi, H.; Katoh, R.; Singh, L. P.; Sugihara, H.; Sayama, K.; Murata, S.; Tachiya, M.; Arakawa, H. *J. Phys. Chem. B* **2002**, *106*, 374−379.
(24) van't Spijker, H.; O'Regan, B.; Goossens, A. *J. Phys. Chem. B* **2001**, *105*, 7220−7226.
(25) Kalyanasundaram, K.; Grätzel, M. *Coord. Chem. Rev.* **1998**, *77*, 347−414.
(26) Redmond, G.; Fitzmaurice, D.; Grätzel, M. *Chem. Mater*. **1994**, *6*, 686−691.
(27) Resmo, H, Keis, K.; Lindström, H.; Södergren, S.; Solbrand, A.; Hagfeldt, A.; Lindquist, S.-E. *J. Phys. Chem. B* **1997**, *101* 2598−2601.
(28) Bedja, I.; Kamat, P. V.; Hua, X.; Lappin, A. G.; Hotchandani, S. *Langmuir* **1997**, *13*, 2398−2403.
(29) Keis, K.; Lindgren, J.; Lindquist, S.-E.; Hagfeldt, A. *Langmuir*, **2000**, *16*, 4688−4694.
(30) Horiuchi, H.; Katoh, R.; Hara, K.; Yanagida, M.; Murata, S.; Sugihara, H.; Arakawa, H.; Tachiya, M. To be published.
(31) Sayama, K.; Sugino, M.; Sugihara, H.; Abe, Y.; Arakawa, H. *Chem. Lett*. **1998**, 753−754.
(32) Hara, K.; Horiguchi, T.; Kinoshita, T.; Sayama, K.; Sugihara, H.; Arakawa, H. *Chem. Lett*. **2000**, 316−317.
(33) Hara, K.; Sato, T.; Tahibana, Y.; Katoh, R.; Furube, A.; Ohga, Y.; Shinpo, A.; Suga, S.; Sayama, K.; Sugihara, H.; Arakawa, H. To be published.
(34) Iwata, K.; Hamaguchi, H. *Appl. Spectrosc*. **1990**, *44*, 1431−1437.
(35) Pankove, J. I. *Optical Processes in Semiconductor*; Dover: New York, 1975.
(36) Yamakata, A.; Ishibashi, T.; Onishi, H. *Chem. Phys. Lett*. **2001**, *333*, 271−277.
(37) Islam, S. D.-M.; Yoshikawa, Y.; Fujitsuka, M.; Watanabe, A.; Ito, O. *Bull. Chem. Soc. Jpn*. **1998**, *71*, 1543−1548.
(38) Weng, Y.-X.; Li, L.; Liu, Y.; Wang, L.; Yang, G.-Z.; Sheng, J.-Q. *Chem. Phys. Lett*. **2002**, *355*, 294−300.
(39) Islam, A.; Hara, K.; Singh, L. P.; Katoh, R.; Yanagida, M.; Murata, S.; Takahashi, Y.; Sugihara, H.; Arakawa, H. *Chem. Lett*. **2000**, 490−491.
(40) Nazeeruddin, Md. K.; Zakeeruddin, S. M.; Humphry-Baker, R.; Jirousek, M.; Liska, P.; Vlachopoulos, N.; Shklover, V.; Fischer, C.-H.; Grätzel, M. *Inorg. Chem*. **1999**, *38*, 6298−6305.
(41) Spitler, M. T. *J. Electroanal. Chem*. **1987**, *78*, 241−250.
(42) Van Houten, J.; Watts, R. J. *J. Am. Chem. Soc*. **1976**, *98*, 4853−4858.
(43) Islam, A.; Sugihara, H.; Singh, L. P.; Hara, K.; Katoh, R.; Nagawa, Y.; Yanagida, M.; Takahashi, Y.; Murata, S.; Arakawa, H. *Inorg. Chim. Acta* **2001**, *322*, 7−16.
(44) Ryan, M. A.; Fitzgerald, E. C.; Spitler, M. T. *J. Phys. Chem*. **1989**, *93*, 6150−6156.
(45) Hashimoto, K.; Hiramoto, M.; Lever, A. B. P.; Sakata, T. *J. Phys. Chem*. **1988**, *92*, 1016−1018.
(46) Sakata, T.; Hashimoto, K.; Hiramoto, M. *J. Phys. Chem*. **1990**, *94*, 3040−3045.
(47) Kavan, L.; Grätzel, M.; Gilbert, S. E.; Klemenz, C.; Scheel, H. J. *J. Am. Chem. Soc*. **1996**, *118*, 6716−6723.
(48) Lu, H. P.; Xie, X. S. *Z. Phys. Chem*. **1999**, *212*, 59−66.
(49) Tachiya, M. *Radiat. Phys. Chem*. **1981**, *17*, 447−456.
(50) Murata, S.; Matsuzaki, S. Y.; Tachiya, M. *J. Phys. Chem*. **1995**, *99*, 5354−5358.
(51) Barzykin, A. V.; Tachiya, M. *J. Phys. Chem*. **2002**, *106*, 4356−4363.
(52) Duffy, N. W.; Peter, L. M.; Rajapakse, R. M. G.; Wijayantha, K. G. U. *Electrochem. Commun*. **2000**, *2*, 658−662.
(53) Kay, A.; Grätzel, M. *J. Phys. Chem*. **1993**, *97*, 6272−6277.
(54) Hagfeldt, A.; Grätzel, M. *Chem. Rev*. **1995**, *95*, 49−68.